

# The internal kinematics of local young stellar associations

## Identifying correlations among age, expansion, rotation, and shear

J. Olivares<sup>1,\*</sup>, N. Miret-Roig<sup>2,3</sup>, and P. A. B. Galli<sup>4</sup>

<sup>1</sup> Departamento de Inteligencia Artificial, Universidad Nacional de Educación a Distancia (UNED), c/Juan del Rosal 16, 28040 Madrid, Spain

<sup>2</sup> Dep. de Física Quàntica i Astrofísica (FQA), Univ. de Barcelona (UB), Martí i Franquès, 1, 08028 Barcelona, Spain

<sup>3</sup> Institut de Ciències del Cosmos (ICCUB), Univ. de Barcelona (UB), Martí i Franquès, 1, 08028 Barcelona, Spain

<sup>4</sup> Instituto de Astronomia, Geofísica e Ciências Atmosféricas, Universidade de São Paulo, Rua do Matão, 1226, Cidade Universitária, 05508-090 São Paulo, SP, Brazil

Received 25 October 2025 / Accepted 30 December 2025

### ABSTRACT

**Context.** The local (<200 pc away) young (<50 Myr old) stellar associations (LYSAs) provide fundamental evidence for the study of the star formation process in the local neighbourhood.

**Aims.** We explore robust statistical correlations in the internal kinematics of LYSAs and of these with age.

**Methods.** We analysed a public dataset containing the linear velocity field parameters and expansion ages of 18 LYSAs. We identified the most robust correlations using frequentist and Bayesian methods.

**Results.** Of the 45 correlations studied, we identified only four that satisfied both frequentist and Bayesian criteria, and all four are related to radial motions in the Galactic Z direction. We hypothesise several origins for these four correlations and identify the gravitational potential of the Galactic disk as the most likely driving element. It imprinted the observed motions in the parent molecular clouds, and once the stars were formed, it also damped these motions on a timescale shorter than the LYSAs' ages.

**Conclusions.** The internal kinematics of LYSAs contain fundamental information about the star formation process that is not fully addressed by star formation theories, in particular rotation and shear. Although the Galactic potential appears to be the driving force of these correlations, we urge the theoretical community to provide predictions about the internal motions of expansion, rotation, and shear of stellar associations.

**Key words.** methods: statistical – stars: kinematics and dynamics – Galaxy: kinematics and dynamics – open clusters and associations: general – solar neighborhood

## 1. Introduction

The young stellar associations in the solar neighbourhood offer an excellent laboratory to study the intrinsic and extrinsic factors affecting the star formation process. Due to their young ages (<50 Myr), they are expected to retain traces of the initial conditions in which they were formed and, thus, provide insight into the dynamics of their star formation process. In addition, their proximity (<200 pc) allows us to disentangle their internal kinematics with unprecedented detail, particularly after the arrival of the exquisite astrometry of the *Gaia* mission (Gaia Collaboration 2016, 2023).

In the *Gaia* era, the internal kinematics of local young stellar associations (LYSAs) have been targeted by several studies (e.g. Wright et al. 2024; Ward & Kruijssen 2018; Kuhn et al. 2019; Galli et al. 2024, 2023, 2021b,a; Gagné & Faherty 2018; Miret-Roig et al. 2025). Most of these studies were limited by either working on the observational space or by transforming spectroscopic radial velocity measurements to the physical space. Recently, Olivares et al. (2025b) published a catalogue with the largest and most homogeneous compilation of internal kinematics and expansion ages of LYSAs. They were obtained via a Bayesian forward-modelling method that infers the internal

kinematics of stellar systems assuming that they follow a linear velocity field (i.e. a first-order Taylor expansion of the velocity field). This catalogue offers the advantage of being homogeneously derived for a set of 18 LYSAs (<200 pc and <50 Myr) whose literature membership lists were unified, cleaned, and scrutinised for the presence of substructures. In this work we employ this catalogue to explore the correlations among the linear velocity field parameters and expansion ages of these LYSAs.

The rest of this work is organised as follows. In Sect. 2, we describe the details of the catalogue. In Sect. 3, we present the classical statistical methods that we used to explore and identify the most prominent correlations. Then, in Sect. 4 we show the results of our statistical exploration, paying particular attention to the age trends that we find in our dataset. In Sect. 5, we discuss the possible origins of these correlations and age trends. Finally, in Sect. 6 we present our conclusions and future work.

## 2. Data

We collected the linear velocity field parameters (see the definition of these parameters in Table 1; for more details, see Sect. 2.3.2 of Olivares et al. 2025a) and expansion ages inferred

\* Corresponding author: jolivares@dia.uned.es

**Table 1.** Parameters of the linear velocity field model.

Symbol	Description
$\kappa_i$	Radial rate along $i$ with $i \in [x, y, z]$
$\omega_i$	Rotation rate along $i$ or in the $\perp_i$ plane, with $i \in [x, y, z]$
$\gamma_i$	Shear rate along $i$ or in the $\perp_i$ plane, with $i \in [x, y, z]$

**Notes.** The linear velocity field parameters are reported in units of  $\text{m s}^{-1} \text{pc}^{-1}$ .

by Olivares et al. (2025b) and reported in their Tables 1 and B.2, respectively. These data correspond to the following young stellar associations:  $\epsilon$ -Chamaeleontis (EPCHA), Musca-Foreground (MuscaFG),  $\eta$ -Chamaeleontis (ETCHA), TW Hydrae A and B (TWA-A and TWA-B), 118 Tau (118TAU), 32 Orionis (THOR),  $\beta$ -Pictoris (BPIC), Octans (OCT), HSC2597, Columba (COL), Carina (CAR), Platais 8, Tucana-Horologium A and B (THA-A and THA-B), and the recently discovered Háap (90 pc,  $25.9 \pm 4.6$  Myr), Balam (63 pc,  $19.3 \pm 4.7$  Myr),  $\omega$ -Aurigae (OMAU; 36 pc,  $40.1 \pm 5.9$  Myr), Nal (183 pc,  $16.1 \pm 5.5$  Myr), and Chem (168 pc,  $22.2 \pm 2.1$  Myr). We note that the Háap association is related to 118TAU and THOR, Balam to BPIC, OMAU to COL, and Nal and Chem to CAR (see Olivares et al. 2025b, for more details). Thus, our dataset contains 200 data points: 10 parameters for each of the 20 groups, with these groups consisting of the 18 LYSA, in which two of them have two substructures.

Figure 1 shows the positions, in Galactic coordinates, of the stellar associations whose data we used in this work. As can be observed, the LYSA are contained within a radius of 200 pc around the Sun and are predominantly skewed towards negative values of  $Y$  and  $Z$ .

Concerning possible biases, we note the following. First, Table B.2 by Olivares et al. (2025b) contains the kinematic parameters inferred from several membership lists of the same stellar systems; thus, to avoid biasing our results from repeating non-independent results of the same stellar system, we only used the parameters corresponding to the final membership selection reported by the authors in their Table 1. Second, although the literature membership lists were cleaned of the most probable binary sources (see Sect. 3.2 of Olivares et al. 2025b), unresolved tight binaries may have influenced the kinematic parameters inferred by the previous authors. However, we notice that the influence of the remaining unresolved binaries can be safely assumed to contribute to the random isotropic increase in the velocity dispersion and thus, their influence on the ordered motions of shear, rotation, and radial expansion or contraction can be assumed to be negligible. Third, here we work with the kinematic parameters inferred by the aforementioned authors based on their linear velocity field model, which, contrary to the Bayesian expansion age model, assumes neither expansion nor contraction and imposes only a weakly informative normal prior on the  $\kappa_i$  parameters (centred at zero with a dispersion of  $100 \text{ m s}^{-1} \text{pc}^{-1}$ ; see Table 1 of Olivares et al. 2025a). Fourth, the spatial distribution of our set of LYSA (see Fig. 1) is restricted to the solar neighbourhood and particularly biased towards the negative sides of the  $Y$  and  $Z$  galactic directions. Thus, the conclusions that may be drawn from this dataset cannot be generalised to the Galactic context nor the extragalactic one. Finally, the age domain of our set of LYSA goes from 7 Myr to 45 Myr, which implies that our conclusions, if any, will need to be reviewed when data from systems younger than 7 Myr and older than 45 Myr are available. We further discuss the implications of these sources of bias in Sect. 5.1.

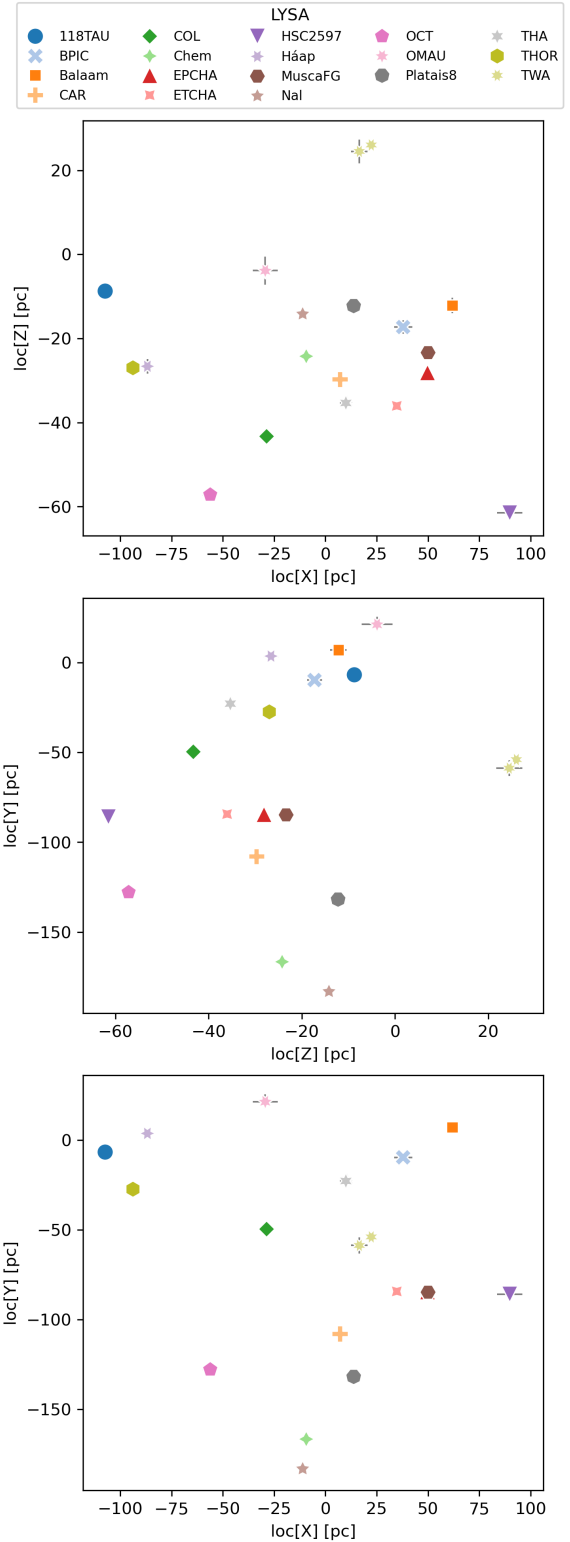


**Fig. 1.** Galactic positions of the LYSA analysed in this work. The symbols and error bars depict the mean and standard deviation of the coordinates' posterior distribution.

### 3. Methods

In this section we present the statistical methods that we used to identify significant correlations and model them. We started by screening the most significant correlations based on Pearson's correlation coefficient and a restrictive p-value threshold. Then,

out of the most significant correlations, we selected the robust ones based on Bayesian and frequentist methods. We note that, given the pioneering origin of this work, our analysis is merely exploratory.

First, we analysed correlations among the parameters of the linear velocity field and the expansion age of the stellar systems using Pearson's correlation coefficient (implemented in the `pearsonr` function within SciPy; Virtanen et al. 2020). We used two-sided null hypothesis tests to discard spurious correlations with p-values larger than  $\alpha = 0.045$ . We assumed, as the null hypothesis, that the underlying distributions of samples are uncorrelated and normally distributed. At this first screening, we did not take into account the uncertainties in the linear velocity field parameters or age. We identified robust correlations as those rejecting the null hypothesis with a confidence of  $2\sigma$  (i.e.  $>95.45\%$ ). In the following, we refer to this method as our frequentist criterion.

Then, we performed a Bayesian hypothesis contrast by modelling the most significant correlations with parametric functions of increasing complexity. We used polynomial models of degree zero (P0) and one (P1) that take into account the uncertainties of the linear velocity field parameters and age (in both coordinates through a bivariate normal likelihood in which the uncertainties enter as the standard deviations in the two-by-two covariance matrix). We also attempted to fit more complex models, like polynomials of degree two and three and an exponential decay for the age correlations, but the dataset lacks the information to constrain the parameters of these more complex models. The use of these nested models, in which the most complex one reduces to the simplest one under certain parameter values (slope zero in this case), allows for a straightforward model comparison. We assumed, as the null hypothesis, the zero-degree polynomial and as the alternative hypothesis the linear one. Thus, we rejected the null hypothesis of no correlation when the 95.45% high-density interval (HDI) of the posterior distribution of the slope parameter does not contain the zero value. In the following, we refer to this method as our Bayesian criterion, and we applied it as a veto step to the frequentist one. As prior distributions for the coefficient parameters, we chose a normal distribution with zero mean and a large standard deviation (50 for the intercept and 10 for the slope, in the corresponding units). This weakly informative distribution centred at zero ensures that the zero value is recovered under no constraining datasets. We fitted the previous models using the Bayesian Python package *PyMC* (Oriol et al. 2023) and analysed the obtained posterior samples with *arviz* (Kumar et al. 2019).

Also, we did a frequentist fit to the data of the identified significant correlations, but this time with a frequentist method. We performed these fits using the `curve_fit` routine from *SciPy* (Virtanen et al. 2020). In these fits, we also incorporated the uncertainties of the linear velocity field parameters and age, although only in the ordinate variable (the only one allowed by this method). However, given that the  $1\sigma$  reported uncertainties are based on a linear approximation to the function model around the optimum (Vugrin et al. 2007), they can be underestimated, and more importantly, the 95.45% HDI cannot be derived from them. For this reason, we restricted our analysis to the HDI obtained from the Bayesian fit described above.

## 4. Results

We applied Pearson's correlation coefficient to each pair of parameters in our dataset (i.e. the nine parameters of the linear velocity field tensor,  $T$ , plus the expansion age). Thus, each

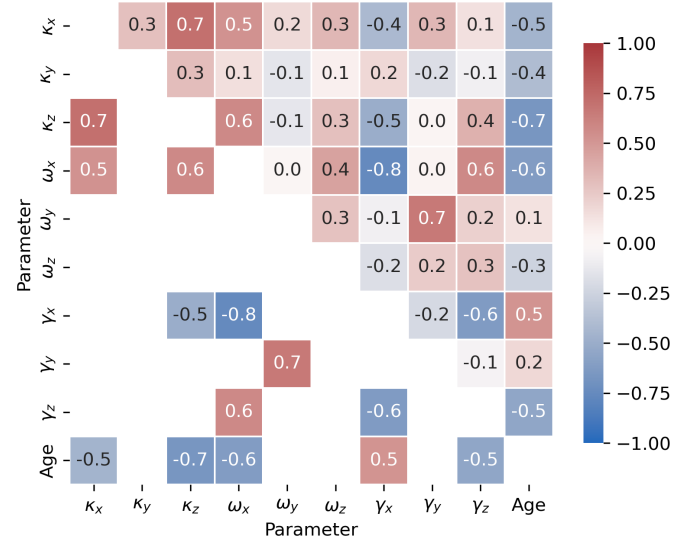


**Fig. 2.** Correlation matrix of the expansion age and linear velocity field parameters for our set of 18 LYSAs. The upper triangular part shows all the correlations, while the lower triangular part shows only those passing our  $2\sigma$  criterion. For the sake of simplicity, the trace is not shown.

of these correlation coefficients is computed with a dataset of 20 points. Then, we discard those correlations deemed as non-significant according to our  $2\sigma$  frequentist criterion. The results of this analysis are summarised in the correlation matrix shown in Fig. 2. In this matrix, the upper triangular part shows all correlations, while the lower triangular part only shows those fulfilling our  $2\sigma$  frequentist criterion. For simplicity, the diagonal (i.e. correlations equal to one) is not shown.

As can be observed from Fig. 2, out of the 45 correlations, only 13 fulfilled our frequentist criterion. If we were to use a more conservative criterion of  $3\sigma$ , only four correlations would have passed it:  $\kappa_x$  versus  $\kappa_z$ ,  $\omega_x$  versus  $\gamma_x$ ,  $\omega_y$  versus  $\gamma_y$ , and  $\kappa_z$  versus age. We consider this  $3\sigma$  criterion to be too restrictive under the current relatively small sample size. For this reason, we stick to our original  $2\sigma$  criterion and, in the following sections, we describe the 13 correlations that survived it. Then, we fitted frequentist and Bayesian polynomial models of degree zero and one to the datasets of these 13 correlations (see Table A.1). Finally, we applied our Bayesian criterion based on the 95.45% HDI of the Bayesian P1 model (the ninth column of the aforementioned table). Out of the 13 frequentist robust correlations, only the following four passed our Bayesian veto criterion:  $\kappa_x$  versus  $\kappa_z$ ,  $\kappa_z$  versus  $\omega_x$ ,  $\kappa_z$  versus  $\gamma_x$ , and  $\kappa_z$  versus age. The details of these correlations are presented throughout the rest of this section.

### 4.1. $\kappa$ correlations

Amongst the  $\kappa$  parameters, only the correlation between  $\kappa_z$  and  $\kappa_x$  passed our frequentist criterion. The sample of data points for these correlations is shown in Fig. 3 together with the Bayesian polynomial models of degree zero (olive lines) and one (orange lines). As can be observed, there is a clear positive linear correlation in the data points that is supported by both criteria (frequentist  $\rho = 0.7$  and slope HDI [0.155, 0.270]). The importance and physical meaning of this correlation will be discussed in Sect. 5.2.

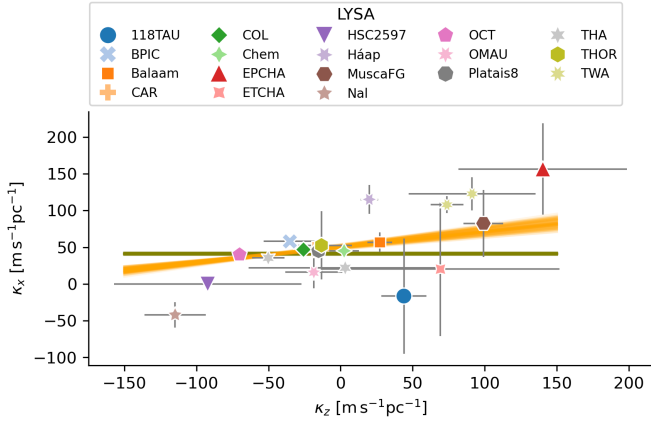


**Fig. 3.** Significant correlations for  $\kappa_z$ . The mean values of the LYSA are shown with coloured symbols and the uncertainties with grey lines. The olive and orange lines show the polynomial fits of degree zero and one, respectively, as obtained from samples of their posterior distributions. We note that THA and TWA have two substructures; thus, their symbols are repeated.

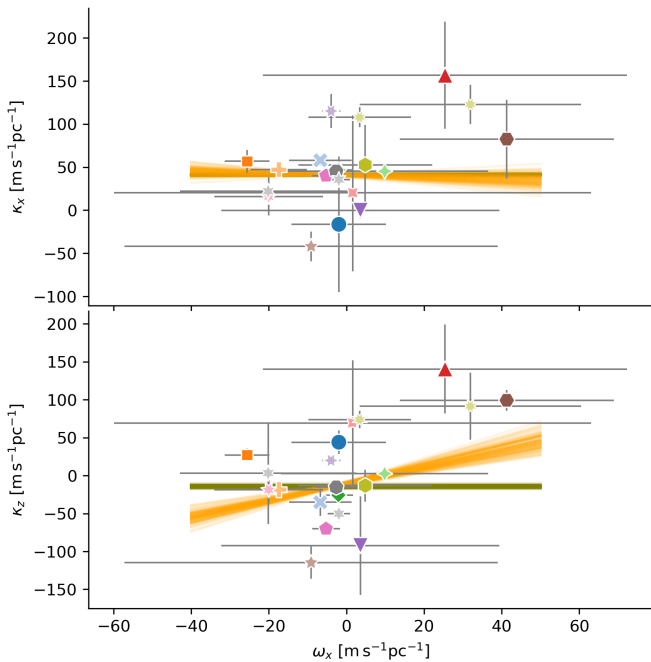


**Fig. 4.** Same as Fig. 3 but for  $\omega_x$ .

#### 4.2. $\omega$ correlations

The frequentist criterion indicates that the rotation of LYSAs is positively correlated with expansion. In particular, the rotation along the  $X$  direction (i.e. in the  $YZ$  plane) is positively correlated with expansion along the  $X$  and  $Y$  directions, with  $\rho=0.5$  and  $\rho=0.6$ , respectively. Figure 4 shows the  $\kappa_x$  and  $\kappa_z$  data as a function of  $\omega_x$  together with the Bayesian polynomials of degree zero (olive lines) and one (orange lines). As can be observed from this figure, only the correlation between  $\kappa_z$  and  $\omega_x$  survived the Bayesian criterion (slope HDI [0.724, 1.514]). The importance and physical meaning of this correlation will be discussed in Sect. 5.3.

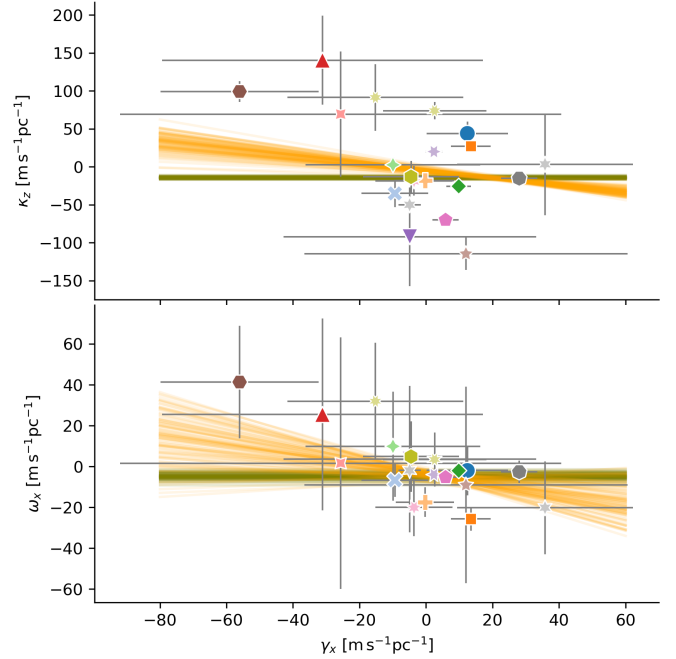


**Fig. 5.** Same as Fig. 3 but for  $\gamma_x$ .

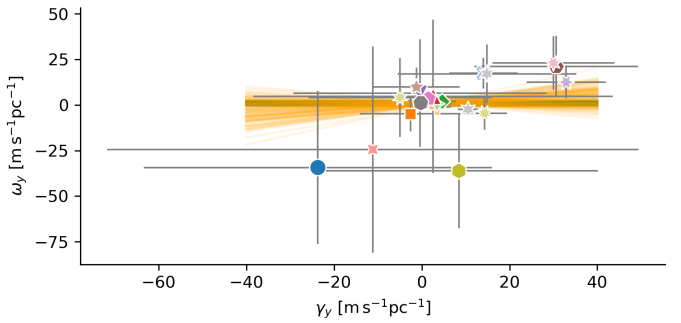


**Fig. 6.** Same as Fig. 3 but for  $\gamma_y$ .

#### 4.3. $\gamma$ correlations

The internal shear motion of LYSAs is strongly correlated with the rest of the linear velocity field parameters. We now describe these correlations, direction by direction.

The shear along the  $X$  direction is negatively correlated with expansion and rotation along the  $Z$  and  $X$  direction, respectively, with frequentist values of  $\rho=-0.5$  and  $\rho=-0.8$ , respectively. The data for these two correlations are shown in Fig. 5 together with the fitted polynomials of degree zero (olive lines) and one (orange lines). As can be observed from this figure, although the mean values (coloured symbols) are indeed negatively correlated, the large uncertainties on  $\gamma_x$  preclude us from drawing stronger conclusions. Indeed, the Bayesian criterion indicates that only in the case of  $\kappa_z$  versus  $\gamma_x$  the correlation is strong (slope HDI [-0.660, -0.255]). We further discuss the importance of this correlation in Sect. 5.4.

The frequentist criterion indicates that the shear along the  $Y$  direction is only strongly correlated ( $\rho=0.7$ ) with the rotation along the same direction. However, as shown in Fig. 6, which contains the data for this correlation as well as the fitted polynomials of degree zero (olive lines) and one (orange lines), this correlation does not survive our Bayesian criterion.

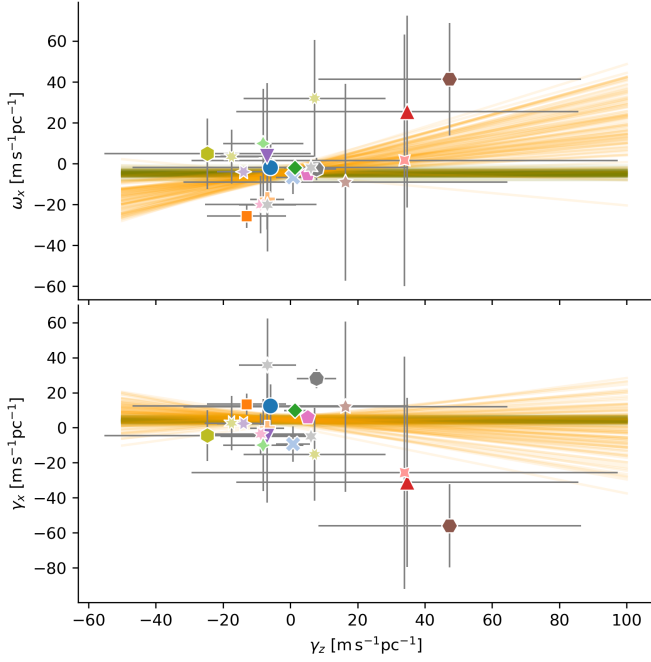


**Fig. 7.** Same as Fig. 3 but for  $\gamma_z$ .

Similar to the previous case, the frequentist criterion specifies that the shear along the Z direction is mildly correlated with the rotation along the X direction ( $\rho=0.6$ ) and mildly anti-correlated with the shear along the X direction ( $\rho=-0.6$ ). However, none of these correlations survived our Bayesian criterion. Figure 7 shows the data points for these correlations as well as the fitted polynomial of degree zero (olive lines) and one (orange lines). As can be observed, in both cases, the polynomials of degree one are compatible with those of degree zero. However, it is worth noticing that in the case of  $\omega_x$  versus  $\gamma_z$ , the slope HDI  $[-0.048, 0.514]$  barely includes zero.

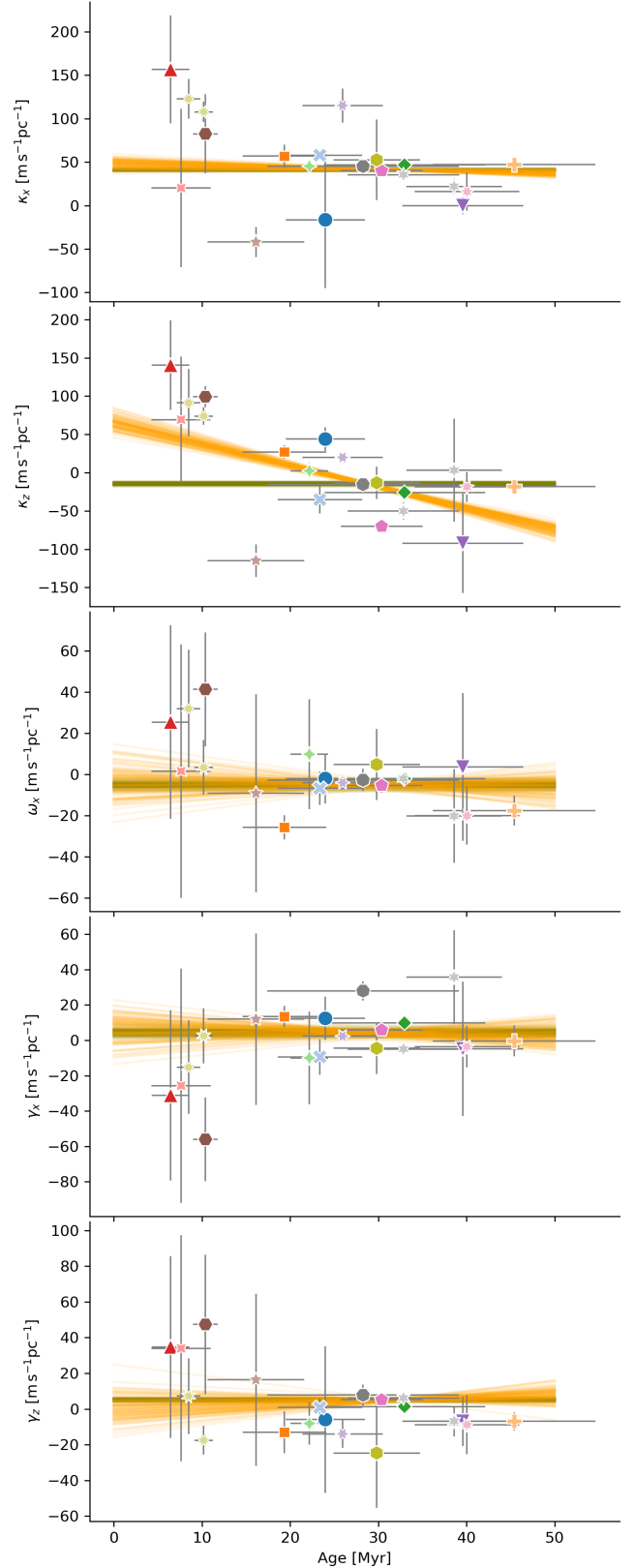
#### 4.4. Age correlations

Figure 8 shows the data for the five age correlations that passed the frequentist criterion together with polynomial fits of degree zero (olive lines) and one (orange lines). As can be observed from this figure, only one of the five correlations survived our Bayesian veto criterion: that of  $\kappa_z$  versus age (slope HDI  $[-3.331, -2.293]$ ). This correlation will be further discussed in Sect. 5.5.

For these five correlations, we attempted to fit an exponential decay, but, in all, except in the case of  $\kappa_x$ , the result was compatible with zero initial value. In the case of  $\kappa_x$  the fitted exponential decay took the following form  $\kappa_x(\text{age}) = 56_{-8}^{+9} e^{(-\text{age}/\tau)} [\text{m s}^{-1} \text{pc}^{-1}]$  with  $\tau = 114_{-53}^{+68}$  Myr. This exponential decay is perfectly compatible with the polynomials of degree zero and one; thus, we prefer to continue working with these simpler models.

## 5. Discussion

In this section, we discuss the statistical and astrophysical relevance of the robust correlations found in the previous section. First, we discuss the possibility that the correlations result from a bias in either the dataset or the methods. Then, we proceed assuming there is no bias and we hypothesise an astrophysical



**Fig. 8.** Same as Fig. 3 but for age.

origin for each type of correlation (i.e.,  $\kappa$ ,  $\omega$ ,  $\gamma$ , and age). Finally, we provide a global astrophysical explanation for their origin and link this explanation to the star formation process.

## 5.1. Possible biases

### 5.1.1. Biased method

False positive discoveries may occur when statistical tests are applied to a single dataset, and only those that are significant are reported. This bias is commonly known as p-hacking or data dredging. Several frequentist corrections are available in the literature to mitigate the presence of false discoveries occurring simply by chance. For example, in our methods, the chosen  $\alpha$  value of 0.045 may result in 4.5% of misclassified correlations (i.e. two pairs of correlations).

To estimate the level of false positives, we applied the false discovery control method by [Benjamini & Hochberg \(2018\)](#). This method returned only six significant correlations, out of the uncorrected 13 originally found, thus indicating that the false discovery rate of the frequentist method is 53%. Assuming conservatively that this false discovery rate can be applied to the results of our set of frequentist plus Bayesian tests, then we conclude that out of our final four correlations, two could be spurious by chance. Therefore, it is of paramount importance that future studies, based on independent datasets, confirm or reject the correlations reported in our exploratory analysis.

### 5.1.2. Biased data

The statistical analysis presented in Sect. 4 shows that the four correlations that satisfied both our frequentist and Bayesian criteria were all linked to  $\kappa_z$ . We do not foresee any possible source of bias in the temporal or spatial (see Fig. 1) domains of our data that may result in the observed correlations of  $\kappa_z$ .

However, exploring the data of  $\kappa_z$  versus  $\kappa_x$ ,  $\omega_x$ ,  $\gamma_x$ , and age (see Figs. 3, 4, 5, and 8, respectively), we observe that the points driving these correlations correspond to the LYSA of EPCHA, ETCHA, MuscaFG, and TWA A and B. With all of them linked to the Scorpius-Centaurus region (Sco-Cen; see e.g. [Miret-Roig et al. 2025](#); [Ratzenböck et al. 2023](#)).

Thus, one possible explanation for the observed correlations with  $\kappa_z$  is that the LYSA in the Sco-Cen region were formed through a peculiar mechanism of star formation that imprinted internal kinematics signatures different from those observed in the rest of the solar neighbourhood. The validation or rejection of this scenario should await the arrival of more constraining datasets, including the rest of the Sco-Cen groups and groups in other star-forming regions of the solar neighbourhood.

We also explored the possibility that spectroscopic binaries that were not flagged as such by the filtering criteria of [Olivares et al. \(2025b\)](#) may bias their catalogue, and as a consequence, our results. Thus, for a subsample of the stellar associations (i.e. CAR, Chem, and OMAU), we removed from their list of members those confirmed as binaries by the literature and inferred their linear velocity field parameters following the method outlined by [Olivares et al. \(2025b\)](#). With the updated catalogue of linear velocity field parameters, we repeated our correlation analysis, finding the same set of robust correlations identified in Sect. 4.

The current dataset does not allow us to further test the bias hypothesis. Thus, in the following we discuss each of the robust correlations assuming that there is no bias in our dataset.

## 5.2. $\kappa$ correlations

The only  $\kappa$  correlation that satisfied both criteria was that of  $\kappa_x$  versus  $\kappa_z$  (see Fig. 3). We notice that this correlation is the strongest that we found, and its strength allowed us to fit

polynomials of orders two and three, with both having non-vanishing coefficients that exclude zero from their posterior 95.45% HDI.

Given the strong and significant  $\kappa$  correlation between the X and Z directions and the low and non-significant correlation that  $\kappa_y$  has with these two directions (see Fig. 2), we hypothesise that some latent force acting on the Z direction (see Sect. 5.6) perturbs the internal radial motions of LYSA (i.e. in  $\kappa_z$ ), and that this perturbation propagates, through a latent mechanism (more in Sect. 5.7), towards  $\kappa_x$ .

## 5.3. $\omega$ correlations

Concerning rotation, the only correlation that satisfied both statistical criteria was that between  $\kappa_z$  and  $\omega_x$ . This correlation means that the rotation observed in the YZ plane is positively correlated with the radial motion (contraction or expansion) in the Z direction. Similar to the case between  $\kappa_z$  versus  $\kappa_x$ , we hypothesise that the rotation in the YZ plane results from a latent force acting on the Z direction (see Sect. 5.6) and producing, through some latent mechanism (more in Sect. 5.7).

## 5.4. $\gamma$ correlations

The only  $\gamma$  correlation that satisfied both our criteria was that between  $\kappa_z$  and  $\gamma_x$ . Given that  $\gamma_x$  indicates a shear motion in the YZ plane, we hypothesise, as in the previous two cases, that a latent force acting preferentially in the Z direction (see Sect. 5.6) results, through some latent mechanism (more in Sect. 5.7), in the shear motion observed in the YZ plane.

## 5.5. Age correlations

As mentioned in Sect. 4.4, only the  $\kappa_z$  versus age correlation passed our two criteria. Although the rest of the correlations did not pass the Bayesian criteria, we briefly discuss them in the following paragraphs.

Concerning the temporal evolution of rotation, to the best of our knowledge, this is the first time that such a large compilation of the Galactic 3D components of rotational signals is analysed for nearby young stellar systems. A similar compilation of rotation signals was recently done by [Jadhav et al. \(2024\)](#). However, those authors worked with the spin projections in the plane of the sky and in the line of sight as measured from radial velocities and proper motions. We notice that those authors find no correlation between the rotation signal and the clusters' age. Here, although we found a strong frequentist correlation between  $\omega_x$  and age, it did not pass our Bayesian criterion. Nonetheless, the patterns observed in Fig. 8 show hints of a temporal decay. The analysis of this decay should await the arrival of more constraining datasets.

Concerning the temporal evolution of shear motions, to the best of our knowledge, this is the first time that such a compilation is presented and analysed. Although according to our Bayesian criterion, none of these shear motions was correlated with age, the data for  $\gamma_x$  and  $\gamma_y$  (see Fig. 8) show hints of a temporal decay. The analysis of this decay should await the arrival of more constraining datasets.

Concerning the temporal evolution of the radial motions (i.e. expansion or contraction), we observe that although both  $\kappa_x$  and  $\kappa_z$  appear to have a similar pattern, only that of  $\kappa_z$  satisfied both our statistical criteria. Despite the statistical significance of the correlation, we notice that the LYSA older than 25–30 Myr have considerably lower expansion than the youngest ones. A

strikingly similar temporal trend was reported by Della Croce et al. (2024) for a considerably larger compilation of stellar systems. However, those authors identify an age decay trend in the ratio of the mean radial velocity to the radial velocity dispersion. According to them, their trend was in agreement with the expectation of violent relaxation and evolution towards virial equilibrium. Although the trend found by those authors is similar to the one observed in our dataset (see e.g. the two upper panels of Fig. 8), we note the following differences. First, we analysed the system's expansion rate vector in Galactic coordinates rather than a radial velocity ratio tied to the observed line of sight. Second, our statistical analysis identifies as robust only the correlation between the system's age and the  $Z$  direction of the expansion. Therefore, although the explanation proposed by the aforementioned authors may hold, an additional external force may still be producing the observed asymmetry in the  $\kappa$  correlations with age, preferentially strengthening the one in the  $Z$  direction. Thus, we hypothesise that the trend observed in Fig. 8, has its origin in a latent force acting on the  $Z$  direction (see Sect. 5.6) that damps the expansion of LYSA's in that direction.

### 5.6. The latent force

As discussed in the previous section, the  $Z$  direction plays a fundamental role in the identified robust correlations. Thus, there should be a latent dynamical variable (i.e. a force) acting in this direction and resulting in the observed correlations. Due to the spatial constraints of our data, this force may have either a local origin or a global one.

Concerning the global origin, we consider that assuming the Galactic potential as the external driving force naturally explains the observed correlations of  $\kappa_z$  (more in Sect. 5.7). The Galactic potential can be safely assumed as the driving force that acts on all LYSA's alike. Moreover, its strongest component, the Galactic disk, acts preferentially on the required  $Z$  direction.

As possible local origins for the driving force, we considered a supernova explosion and a local gravitational perturbation. On the one hand, a supernova explosion at high  $Z$  may result in a shock wave with an almost parallel front to the Galactic plane that may have compressed the molecular clouds in the  $Z$  direction and thus resulted, through some hidden mechanism (more in Sect. 5.7), in the observed kinematic patterns and correlations. On the other hand, the possibility of a local gravitational perturbation is currently discarded from the results by Widmark et al. (2021). These authors infer the gravitational potential of the Galactic disk in the solar neighbourhood using a Bayesian hierarchical model and *Gaia* Data Release 2 data. Their results indicate (see their Fig. 7 for  $Z$  within 100 pc) that, at the spatial distribution of our data ( $X \in [-100, 100]$  pc,  $Y \in [-200, 50]$  pc, and  $Z \in [-60, 30]$  pc; see Fig. 1), the inferred gravitational potential is homogeneous and similar to that of the rest of the solar neighbourhood (within an XY radius of 200 pc and  $Z$  within 100 pc). We notice that there is a large perturbation in the gravitational potential inferred by the previous authors (see region A4 in their Fig. 8). However, this perturbation occurs at high Galactic altitude ( $Z = 400$  pc).

The hypothesis of a local origin for the force acting in the  $Z$  direction lacks constraining evidence. Thus, in the following, we assume that this force has a global origin and that it corresponds to the force exerted by the Galactic disk.

### 5.7. The latent mechanism

Under the assumptions that our data are not biased, that the internal kinematics of LYSA's associated with Sco-Cen are not

different from those of other LYSA's in the solar neighbourhood, and that the latent force acting in the  $Z$  direction corresponds to that of the gravitational potential of the Galactic disk, we are now faced with the question about the physical latent mechanism that transforms the previous force into the observed statistical correlations of  $\kappa_z$  with age, expansion, rotation, and shear.

This latent mechanism should relate the force in the  $Z$  direction (i.e. the gravitational potential of the Galactic disk) with expansion in the  $X$  direction, rotation in the  $YZ$  plane, and shear in the  $YZ$  plane. In addition, this same mechanism or another one must explain the temporal decay of expansion, rotation, and shear in a timescale of 20–30 Myr.

We considered three not necessarily independent mechanisms for the origin of the  $\kappa_z$  correlations. In the first one, which we call the hereditary mechanism, the correlations were already present in the parent molecular cloud and were simply inherited by the newborn stars. In the second one, which we call the nourishing mechanism, the kinematic correlations were created at the birth time of the associations as a by-product of the star formation process (see e.g. Mapelli 2017; Lahén et al. 2020, and references there in). Finally, in the third mechanism, the correlations resulted from dynamical interactions of the newly formed stars among themselves and with the Galactic potential. However, we consider this third mechanism unfeasible due to the young ages, unbound state, and collisionless nature of stellar associations. Moreover, this third mechanism is ruled out by the results shown in Sect. 4.4, in which expansion, rotation, and shear decrease rather than increase with age. We now explore the feasibility of the remaining two mechanisms.

In the hereditary mechanism, the molecular clouds, which can be considered classical collisional fluids, acquired the rotation and shear motions due to the Galactic potential, while the radial motions of contraction and expansion (in all directions) may result from their own gravitational collapse. Their viscosity allows them to react, under a compressing force in the  $Z$  direction, with shear motions in the  $XZ$  and  $YZ$  planes, and in turn, these shear motions will result in local vorticity, and thus rotation. This hereditary mechanism is favoured by the observational evidence of the Milky Way and other galaxies. In the Milky Way, the observed vertical velocity gradient,  $-15 \pm 4 \text{ m s}^{-1} \text{ pc}^{-1}$  (Marasco & Fraternali 2011), is expected to produce shear motions in the  $XZ$  and  $YZ$  planes, and thus, also vorticity. We notice that the value of this vertical velocity gradient is similar to the observed shear motions of the youngest LYSA's (see  $\gamma_x$  vs age in Fig. 8). In other galaxies, the rotational signals of molecular clouds (measured in the plane of the sky) have values also similar to those observed in our LYSA's (see  $\omega_x$  vs age in Fig. 8):  $6\text{--}8 \text{ m s}^{-1} \text{ pc}^{-1}$  in M33 (Braine et al. 2018) and  $18\text{--}22 \text{ m s}^{-1} \text{ pc}^{-1}$  in M51 (Braine et al. 2020).

In the nourishing mechanism, the parent molecular cloud fragments into smaller clumps that afterwards assemble hierarchically with a mass-dependent relation (Mapelli 2017; Lahén et al. 2020). This hierarchical assembling produces rotation as a consequence of torques between clumps (e.g. Mapelli 2017) or as a direct consequence of the star formation at the merger of two dwarf galaxies (Lahén et al. 2020). This mechanism faces several difficulties in explaining the observed correlations with  $\kappa_z$ . First, the numerical simulations by Lahén et al. (2020) and Mapelli (2017) indicate that rotation is observed in massive and compact stellar systems while it is elusive in the least massive and sparse systems like stellar associations (see e.g. the discussion in Mapelli 2017, about their run D). Second, although shear motions are not directly mentioned in any of the previous works, they are also expected to appear from the torques between

gaseous clumps. Third, the random nature of the turbulent flows that give birth to the clumps veils the explanation for the correlations of rotation and shear with expansion. For these correlations to appear, the torques between clumps must preferentially occur in the YZ plane. Although this asymmetry may arise from the presence of the Galactic disk potential, the previous simulations do not include it.

Most likely, the previous two mechanisms operate simultaneously. Nonetheless, once the stellar system was formed and imprinted with the observed kinematic patterns of expansion, rotation, and shear, these vanish in a timescale of 20–30 Myr. Concerning expansion, we expect that this motion will face differential forces due to the Galactic potential, with the latter preferentially damping the motion in the Z direction. Nonetheless, we expect that other phenomena, like violent relaxation and evolution towards virial equilibrium, also play important roles (e.g. Della Croce et al. 2024). Concerning rotation, the numerical simulations by Bissekenov et al. (2025) predict that the initial bulk rotation signal will disappear on the timescale of two-body relaxation, which for stellar associations is larger than their age. However, our data show (see Fig. 4.4) that the initial rotation vanishes after only 20–30 Myr. Thus, other mechanisms not included in the previous authors’ simulations must be at play. In particular, we note that their simulations used the tidal field created by a point mass galaxy, whereas in the case of the solar neighbourhood, the most important contribution to the gravitational field comes from the Galactic disk. Thus, we hypothesise that the disk is responsible for the damping of stellar motions in the Z direction, particularly those of rotation and shear in the YZ plane and expansion in the Z direction.

## 6. Conclusions

In this work, we identified the most robust statistical correlations in the internal kinematics of LYSAs. Using a recently published catalogue with the linear velocity field parameters and expansion ages of 18 LYSAs, we searched for the most robust ( $2\sigma$  credible) correlations using frequentist and Bayesian criteria. Only four of the 45 correlations satisfied both statistical criteria; these are  $\kappa_x$  versus  $\kappa_z$ ,  $\kappa_z$  versus  $\omega_x$ ,  $\kappa_z$  versus  $\gamma_x$ , and  $\kappa_z$  versus age, which are shown in Fig. 9. We estimate a false discovery rate of 53%, which indicates that at least two of the reported robust correlations could be coincidental. The confirmation of the true robust correlations will require future confirmatory studies based on independent datasets. The found robust correlations are all related to expansion in the Z direction (i.e.  $\kappa_z$  versus age, expansion, rotation, and shear), and thus, the most probable physical explanation is that they are due to the gravitational potential of the Galactic disk.

Given the lack of theoretical predictions about the internal motions of sparse stellar systems such as stellar associations, we have proposed several explanations for the observed robust correlations. We find that the most probable driving element corresponds to the force exerted by the gravitational potential of the Galactic disk. While this later imprints rotation and shear motions in the parent molecular clouds, expansion results as a by-product of the star formation process due to the gravitational collapse of these parent clouds. Once the stars are formed, the same Galactic potential that originates the internal motions damps them on timescales shorter than the LYSAs’ ages.

The confirmation of this scenario still awaits the arrival of larger samples of stellar systems, particularly those in nearby star-forming regions and large local complexes (e.g. Sco-Cen

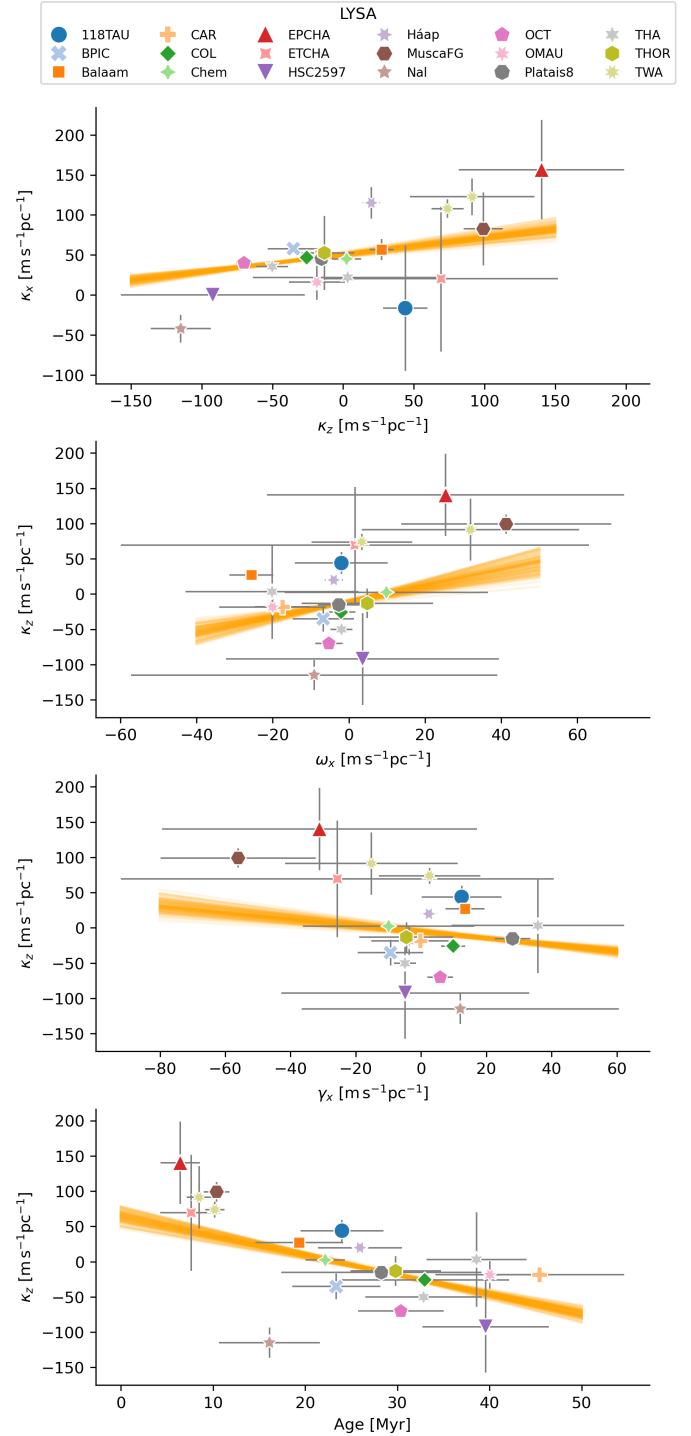


**Fig. 9.** Summary of the identified robust correlations. The symbols and grey bars depict the mean and standard deviations of the parameter values of LYSAs inferred by Olivares et al. (2025b), while the orange lines show samples of the posterior distribution of the linear fit (degree-one polynomial) inferred in this work.

and Taurus-Auriga). Analysing larger samples of stellar associations, particularly those within the large complexes, will be of paramount importance to disentangle global correlations from those arising at smaller scales due to peculiar star formation histories. In addition, future work will also be needed to develop more sophisticated models for the observed robust correlations.

*Acknowledgements.* We thank the anonymous referee for the useful comments that helped to improve the quality of this work. JO acknowledge financial support from ‘Ayudas para contratos postdoctorales de investigación UNED 2021’. ‘La publicación es parte del proyecto PID2022-142707NA-I00, financiado por MCIN/AEI/10.13039/501100011033/FEDER, UE’. NMR acknowledges support from the Beatriu de Pinós postdoctoral program under the Ministry of Research and Universities of the Government of Catalonia (Grant Reference No. 2023 BP 00215). P.A.B.G. acknowledges financial support from the São Paulo Research Foundation (FAPESP, grant: 2020/12518-8) and Conselho Nacional de Desenvolvimento Científico e Tecnológico (CNPq, grant: 303659/2024-6).

## References

- Benjamini, Y., & Hochberg, Y. 2018, *J. Roy. Statist. Soc. Ser. B (Methodol.)*, **57**, 289
- Bissekenov, A., Pang, X., Kamlah, A., et al. 2025, *A&A*, **699**, A196
- Braine, J., Rosolowsky, E., Gratier, P., Corbelli, E., & Schuster, K. F. 2018, *A&A*, **612**, A51
- Braine, J., Hughes, A., Rosolowsky, E., et al. 2020, *A&A*, **633**, A17
- Della Croce, A., Dalessandro, E., Livernois, A., & Vesperini, E. 2024, *A&A*, **683**, A10
- Gagné, J., & Faherty, J. K. 2018, *ApJ*, **862**, 138
- Gaia Collaboration (Prusti, T., et al.) 2016, *A&A*, **595**, A1
- Gaia Collaboration (Vallenari, A., et al.) 2023, *A&A*, **674**, A1
- Galli, P. A. B., Bouy, H., Olivares, J., et al. 2021a, *A&A*, **654**, A122
- Galli, P. A. B., Bouy, H., Olivares, J., et al. 2021b, *A&A*, **646**, A46
- Galli, P. A. B., Miret-Roig, N., Bouy, H., Olivares, J., & Barrado, D. 2023, *MNRAS*, **520**, 6245
- Galli, P. A. B., Miret-Roig, N., Bouy, H., Olivares, J., & Barrado, D. 2024, *A&A*, **689**, A11
- Jadhav, V. V., Kroupa, P., Wu, W., Pflamm-Altenburg, J., & Thies, I. 2024, *A&A*, **687**, A89
- Kuhn, M. A., Hillenbrand, L. A., Sills, A., Feigelson, E. D., & Getman, K. V. 2019, *ApJ*, **870**, 32
- Kumar, R., Carroll, C., Hartikainen, A., & Martín, O. 2019, *J. Open Source Softw.*, **4**, 1143
- Lahén, N., Naab, T., Johansson, P. H., et al. 2020, *ApJ*, **904**, 71
- Mapelli, M. 2017, *MNRAS*, **467**, 3255
- Marasco, A., & Fraternali, F. 2011, *A&A*, **525**, A134
- Miret-Roig, N., Alves, J., Ratzenböck, S., et al. 2025, *A&A*, **694**, A60
- Olivares, J., Bouy, H., Dorn-Wallenstein, T. Z., & Berihuete, A. 2025a, *A&A*, **693**, A12
- Olivares, J., Miret-Roig, N., Galli, P. A. B., & Bouy, H. 2025b, *A&A*, **699**, A122
- Oriol, A.-P., Virgile, A., Colin, C., et al. 2023, *PeerJ Comput. Sci.*, **9**, e1516
- Ratzenböck, S., Großschedl, J. E., Möller, T., et al. 2023, *A&A*, **677**, A59
- Virtanen, P., Gommers, R., Oliphant, T. E., et al. 2020, *Nat. Methods*, **17**, 261
- Vugrin, K. W., Swiler, L. P., Roberts, R. M., Stucky-Mack, N. J., & Sullivan, S. P. 2007, *Water Resour. Res.*, **43**, <https://agupubs.onlinelibrary.wiley.com/doi/pdf/10.1029/2005WR004804>
- Ward, J. L., & Kruijssen, J. M. D. 2018, *MNRAS*, **475**, 5659
- Widmark, A., de Salas, P. F., & Monari, G. 2021, *A&A*, **646**, A67
- Wright, N. J., Jeffries, R. D., Jackson, R. J., et al. 2024, *MNRAS*, **533**, 705

## Appendix A: Additional tables

Table A.1. Parameters of the polynomial fits of degree zero (P0) and one (P1).

Correlation	Model	Case	Intercept			Slope		
			mu	sd	HDI	mu	sd	HDI
$\kappa_x$ vs $\kappa_z$	P0	Bayesian	41.14	0.77	[39.631,42.705]	-	-	
		Frequentist	41.15	0.77		-	-	
	P1	Bayesian	50.45	1.48	[47.436,53.371]	0.21	0.03	[0.155,0.270]
		Frequentist	50.50	1.49		0.21	0.03	
$\kappa_x$ vs $\omega_x$	P0	Bayesian	41.13	0.75	[39.587,42.608]	-	-	
		Frequentist	41.15	0.77		-	-	
	P1	Bayesian	40.76	0.96	[38.909,42.753]	-0.08	0.12	[-0.323,0.175]
		Frequentist	40.78	0.95		-0.08	0.12	
$\kappa_z$ vs $\omega_x$	P0	Bayesian	-14.38	1.40	[-17.126,-11.542]	-	-	
		Frequentist	-14.39	1.39		-	-	
	P1	Bayesian	-10.67	1.56	[-13.744,-7.501]	1.11	0.20	[0.724,1.514]
		Frequentist	-10.69	1.54		1.11	0.20	
$\kappa_z$ vs $\gamma_x$	P0	Bayesian	-14.38	1.40	[-17.080,-11.439]	-	-	
		Frequentist	-14.39	1.39		-	-	
	P1	Bayesian	-5.52	2.38	[-10.112,-0.506]	-0.46	0.10	[-0.660,-0.255]
		Frequentist	-5.59	2.35		-0.46	0.10	
$\omega_x$ vs $\gamma_x$	P0	Bayesian	-4.86	1.33	[-7.483,-2.197]	-	-	
		Frequentist	-4.86	1.32		-	-	
	P1	Bayesian	-3.99	1.43	[-6.870,-1.188]	-0.23	0.14	[-0.529,0.046]
		Frequentist	-3.99	1.43		-0.23	0.15	
$\omega_y$ vs $\gamma_y$	P0	Bayesian	0.96	0.78	[-0.569,2.522]	-	-	
		Frequentist	0.97	0.76		-	-	
	P1	Bayesian	0.74	0.90	[-1.005,2.526]	0.07	0.14	[-0.203,0.365]
		Frequentist	0.74	0.90		0.07	0.14	
$\omega_x$ vs $\gamma_z$	P0	Bayesian	-4.87	1.31	[-7.558,-2.263]	-	-	
		Frequentist	-4.86	1.32		-	-	
	P1	Bayesian	-4.15	1.40	[-6.806,-1.294]	0.25	0.14	[-0.048,0.514]
		Frequentist	-4.16	1.38		0.25	0.14	
$\gamma_x$ vs $\gamma_z$	P0	Bayesian	4.35	1.39	[1.707,7.223]	-	-	
		Frequentist	4.39	1.42		-	-	
	P1	Bayesian	4.32	1.50	[1.223,7.244]	-0.02	0.14	[-0.299,0.274]
		Frequentist	4.31	1.49		-0.03	0.14	
$\kappa_x$ vs Age	P0	Bayesian	41.14	0.76	[39.649,42.690]	-	-	
		Frequentist	41.15	0.77		-	-	
	P1	Bayesian	49.19	4.22	[40.547,57.594]	-0.25	0.13	[-0.511,0.005]
		Frequentist	49.49	4.22		-0.26	0.13	
$\kappa_z$ vs Age	P0	Bayesian	-14.40	1.40	[-17.337,-11.683]	-	-	
		Frequentist	-14.39	1.39		-	-	
	P1	Bayesian	65.36	7.52	[49.761,79.702]	-2.80	0.26	[-3.312,-2.277]
		Frequentist	66.97	7.69		-2.86	0.27	
$\omega_x$ vs Age	P0	Bayesian	-4.88	1.31	[-7.429,-2.216]	-	-	
		Frequentist	-4.86	1.32		-	-	
	P1	Bayesian	-3.21	6.92	[-16.956,10.051]	-0.06	0.23	[-0.522,0.389]
		Frequentist	-3.62	7.07		-0.04	0.24	
$\gamma_x$ vs Age	P0	Bayesian	4.41	1.43	[1.646,7.347]	-	-	
		Frequentist	4.39	1.42		-	-	
	P1	Bayesian	6.43	7.49	[-9.089,21.067]	-0.07	0.25	[-0.585,0.434]
		Frequentist	6.59	7.66		-0.08	0.26	
$\gamma_z$ vs Age	P0	Bayesian	5.11	0.59	[3.952,6.300]	-	-	
		Frequentist	5.11	0.60		-	-	
	P1	Bayesian	-0.64	6.21	[-12.246,11.816]	0.18	0.19	[-0.212,0.539]
		Frequentist	-1.08	6.28		0.19	0.19	